Core-Hole Excitation Spectra of the Oxides and Hydrates of Fullerene C_{60} and Azafullerene $C_{59}N$

Xiong Li [1,2], Shuyi Wang [1,3], Jingdong Guo [3], Ziye Wu [4], Changrui Guo [4], Shaohong Cai [4,5,*] and Mingsen Deng [4,*]

[1] College of Big Data and Information Engineering, Guizhou University, Guiyang 550025, China; lix@ecut.edu.cn (X.L.); shuyiwang@gznc.edu.cn (S.W.)
[2] School of Science, East China University of Technology, Nanchang 330013, China
[3] Guizhou Provincial Key Laboratory of Computational Nano-Material Science, Guizhou Education University, Guiyang 550018, China; jingdongguo@126.com
[4] School of Information, Guizhou University of Finance and Economics, Guiyang 550025, China; zywu@mail.gufe.edu.cn (Z.W.); guochangrui@mail.gufe.edu.cn (C.G.)
[5] Department of Resources and Environment, Moutai Institute, Renhuai 564507, China
[*] Correspondence: caish@mail.gufe.edu.cn (S.C.); msdeng@mail.gufe.edu.cn (M.D.)

Abstract: The interaction of fullerenes and their derivatives with environmental molecules such as oxygen or water was crucial for the rational design of low-dimensional materials and devices. In this paper, the near-edge X-ray absorption fine structure (NEXAFS), X-ray emission spectroscopy (XES) and X-ray photoelectron spectroscopy (XPS) shake-up satellites were employed to distinguish the oxides and hydrates of the fullerene C_{60} and azafullerene $C_{59}N$ families. The study includes various isomers, such as the open [5,6] and closed [6,6] isomers of $C_{60}O$, $C_{60}H(OH)$, C_{60}-O-C_{60}, $C_{60}H$-O-$C_{60}H$, $C_{59}N(OH)$ and $C_{59}N$-O-$C_{59}N$, based on density functional theory. These soft X-ray spectra offered comprehensive insights into the molecular orbitals of these azafullerene molecular groups. The oxygen K-edge NEXAFS, carbon and oxygen K-edge XPS shake-up satellite spectra provided valuable tools for distinguishing oxides or hydrates of fullerene C_{60} and azafullerene $C_{59}N$. Our findings could significantly benefit the development of fullerene functional molecular materials and expand the application scope of soft X-ray spectroscopy as a molecular fingerprinting tool for the fullerene family.

Keywords: azafullerene; oxide; hydrate; NEXAFS; XES; XPS shake-up

1. Introduction

The carbon allotrope fullerene C_{60} and its molecular crystals are considered fundamental units in probing the mechanisms of transport and photoelectric processes. Their fast carrier mobility and strong electron affinity position fullerenes are at the forefront of electronic device applications, including field-effect transistors [1] or photovoltaics [2], nanomedicine [3], nanoelectronics [4], organic and inorganic nanocomposites [5,6]. The azafullerene $C_{59}N$ monomer, notable for its unpaired electrons and resultant free radical behavior [7], remains a vibrant research area despite its instability. For example, the report of Martín-Gomis et al. showed promising implications in the development of organic solar cells built with covalent donor-acceptor systems using $C_{59}N$ as the acceptor [8]. Further, the $C_{59}N$ system has been shown to achieve a more persistent charge-separated state [9], underscoring its potential in advanced applications.

However, the insertion of extrinsic species, such as oxygen and water, could substantially alter the physical properties of these electronic materials [10]. Numerous studies have reported evidence for the sensitivity of fullerene or azafullerene to the incorporation of such impurities [11–14]. To further understand these impacts, Lin et al. conducted a detailed study on the oxidation process of azafullerene $C_{59}N$ [15]. Research has established that
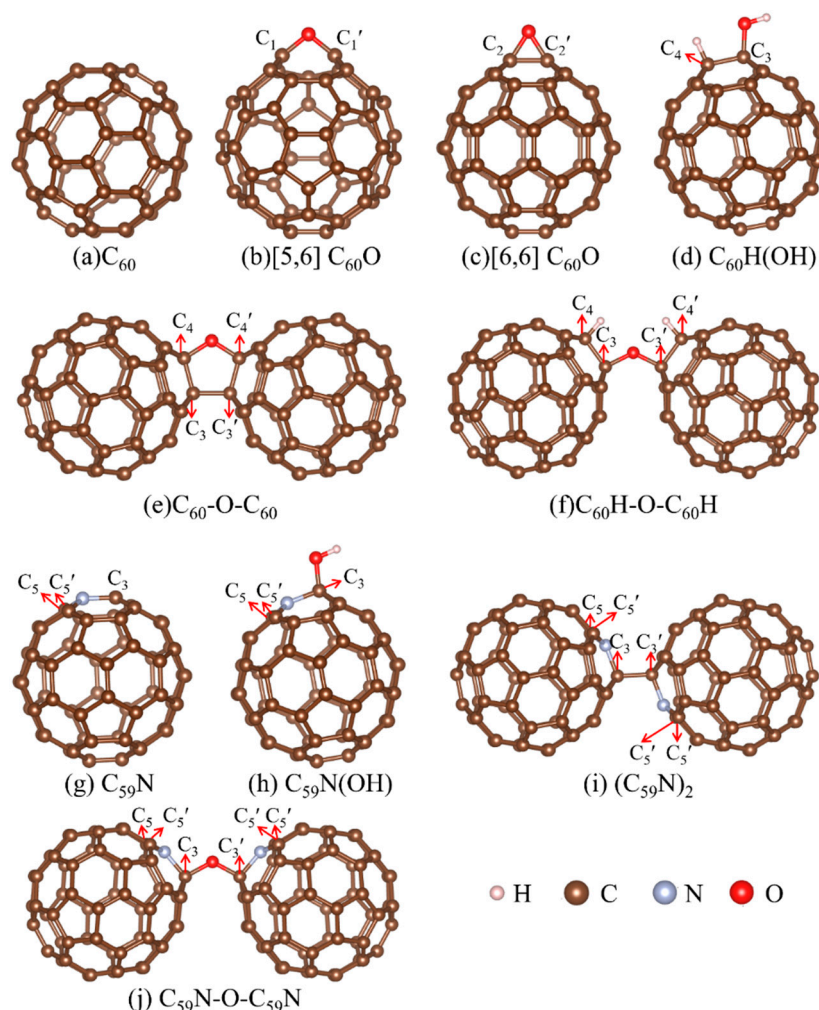
oxides and hydrates of fullerene and azafullerene are key materials in constructing a variety of fullerene-based nanostructures [16,17]. As a straightforward derivative of fullerene, $C_{60}O$ has emerged as a foundational material for producing more complex fullerene oxides, playing a crucial role in the synthesis of diverse compounds [18–20]. Fedurco et al. and Jones et al. demonstrated that $N@C_{60}O$ represented a valuable intermediary for researchers engaged in quantum information processing at the molecular level [21]. The work of Mondal et al. has also highlighted the complex interplay between thermal and mechanical transformations within the $C_{60}O$ cluster, which could influence its thermoelectric properties through the modulation of intermolecular interactions [22]. Moreover, the $C_{59}N$ oxides have been identified as robust recyclable catalysts, featuring a rate-determining energy barrier of 0.80 eV [23].

The presence of oxides and water-related reactions in fullerene and azafullerene compounds often leads to substantial modifications in the physical properties of organic semiconductors. These modifications are instrumental in the fabrication of numerous fullerene nanostructures. However, the properties of the oxides and hydrates exhibit significant variations [18]. Consequently, understanding their electronic and chemical characteristics is essential for further exploration and utilization. In this regard, Palotás et al. have made a noteworthy contribution by providing the initial experimental infrared multiple-photon dissociation vibrational spectra of gaseous $C_{60}O^+$ and $C_{60}OH^+$. However, challenges persist, as the experimental band centered at 1333 cm^{-1} was not accurately reproduced by the theoretical $[6,6]C_{60}OH^+$ spectrum [24]. This discrepancy demands considerable efforts dedicated to acquiring a deeper understanding of these materials, as evident in the studies mentioned earlier [25–28], where X-ray spectra have proven to be valuable experimental methods for investigating the electronic structures of aza[60]fullerene [29–31].

Near-edge X-ray absorption fine structure (NEXAFS) is a well-established spectroscopic approach employed for examining the local molecular structure and acquiring insights into unoccupied molecular orbitals. X-ray emission spectroscopy (XES) was frequently utilized to investigate the occupancy density of molecular electronic states. Both NEXAFS and XES offered element and site-specific capabilities, making them potent tools for elucidating intricate electronic properties of materials. Additionally, X-ray photoelectron spectroscopy (XPS) shake-up satellites, engendered by excitations of valence electrons concomitant with the ionization of core electrons, provided information regarding the valence band of materials in the vicinity of the core-hole screening [32–39]. For instance, Klein et al. utilized the delta-self-consistent-field (ΔSCF) and transition potential (TP) methods for calculating XPS and NEXAFS transitions, allowing the prediction of *K*-shell information [40]. Meanwhile, Armillotta et al. investigated the mechanisms of metal intermolecular coordination using NEXAFS technology [41].

The open [5,6] and closed [6,6] isomers of $C_{60}O$, as well as C_{60}-O-C_{60}, are examples of molecular crystals that had been synthesized [42–44]. Creegan et al. identified the epoxide isomer of $C_{60}O$ through ^{13}C NMR and FTIR examinations, revealing that the oxygen atom bridges to carbon atoms of two hexagons with C_{2v} symmetry [42]. Weisman et al. further demonstrated that $C_{60}O$ can be prepared in both closed [6,6] epoxide and open [5,6] annulene isomers, depending on the synthesis method [44]. The C_{60}-O-C_{60} molecular crystal consists of a C_{60} dimer, and an oxygen atom bridged in a furan-like ring (Figure 1e) [43], while the two isomers of $C_{60}O$ are composed of a C_{60} monomer and an oxygen atom in the form of epoxide and annulene, respectively (Figure 1b,c) [42]. Erbahar et al. discovered that the most stable structure for a single oxygen atom within $(C_{59}N)_2$ involves the oxygen atom in an ether configuration, forming a cross-linking bond between two $(C_{59}N)$ units [45], namely $C_{59}N$-O-$C_{59}N$ (Figure 1j). In the reaction between H_2O and C_{60}, the configuration of the cross-linking bond could also be considered, specifically $C_{60}H$-O-$C_{60}H$ (Figure 1f). In this study, the NEXAFS, XES and XPS shake-up satellites for seven exemplary members of the hydrates and oxides of fullerene C_{60} and aza[60]fullerene $C_{59}N$, namely open [5,6] and closed [6,6] isomers of $C_{60}O$, $C_{60}H(OH)$, C_{60}-O-C_{60}, $C_{60}H$-O-$C_{60}H$, $C_{59}N(OH)$ and $C_{59}N$-O-$C_{59}N$, were studied by employing the full core-hole

(FCH) potential method as well as equivalent core-hole Kohn–Sham (ECH-KS) approach. The study provides valuable insights that can support and guide further experimental investigations related to these oxide materials and water-involved reactions.

Figure 1. The optimized molecular models of the fullerene C_{60}, aza[60]fullerene $C_{59}N$, their oxides, and hydrates, the carbon atoms C_1 and C_1', C_2 and C_2', C_3 and C_3', C_4 and C_4' and C_5 and C_5' are symmetrically equivalent.

2. Results and Discussion

The optimized molecular models of the fullerene C_{60}, aza[60]fullerene $C_{59}N$, their oxides and hydrates are shown in Figure 1. The carbon atoms C_1 and C_1', C_2 and C_2', C_3 and C_3', C_4 and C_4' and C_5 and C_5' are symmetrically equivalent. The binding energies (BE) of the H atom, O atom, OH, $C_{59}N$, and C_{60} to the $C_{59}N$ and C_{60} monomers were calculated to obtain the stability of oxides and hydrates of the fullerenes and azafullerenes by

$$E_{BE} = E_{tot} - \sum_{i=1}^{n} E_i \qquad (1)$$

where E_{tot} is the electronic energy of C_{60}, open [5,6] and closed [6,6] isomers of $C_{60}O$, $C_{60}H(OH)$, C_{60}-O-C_{60}, $C_{60}H$-O-$C_{60}H$, $C_{59}N$, $C_{59}N(OH)$, $(C_{59}N)_2$ and $C_{59}N$-O-$C_{59}N$ molecules, E_i is the electronic energy of the isolated H atom, O atom, OH, $C_{59}N$ and C_{60} molecule, which are the monomers that constitute the ten molecules mentioned above. HOMO-LUMO energy gap (E_{gap}) is calculated by

$$E_{gap} = E_{LUMO} - E_{HOMO} \qquad (2)$$

where E_{LUMO} are LUMO energies and E_{HOMO} are HOMO energies. The binding energies, HOMO and LUMO energies and E_{gap} are collected in Table 1, which are verified well with the theoretical investigations based on the B3LYP [46] and LDA-PW91 [45] level. The symmetry point groups and the number of symmetrically inequivalent carbon atoms for the ten molecule groups are also shown in Table 1. The energy gaps decrease upon oxidation and hydration of fullerene C_{60}, whereas the gaps increase for azafullerene $C_{59}N$. The energy gap change trends indicated that the fullerene C_{60} becomes more reactive after oxidation and hydration, while azafullerene $C_{59}N$ becomes less reactive after oxidation and hydration. The binding energies confirm that these oxides and hydrates are more stable than the $(C_{59}N)_2$ molecule, with the $C_{60}H$-O-$C_{60}H$ molecule identified as the most stable oxidation configuration.

Table 1. Binding energies calculated using the B3LYP/6-31G(d,p) level, HOMO and LUMO energies, E_{gap}, symmetry point groups and the number of symmetrically inequivalent carbon atoms for the fullerene C_{60}, aza[60]fullerene $C_{59}N$, their oxides and hydrates.

Molecule	HOMO Energy (eV)	LUMO Energy (eV)	E_{gap} (eV)	BE (kcal/mol)	Sym.	Number of Symmetrically Inequivalent Carbon
C_{60}	−5.99	−3.23	2.76	−	I_h	1
$[5,6]C_{60}O$	−5.90	−3.30	2.60	−78.92	C_s	32
$[6,6]C_{60}O$	−5.94	−3.33	2.61	−76.81	C_{2v}	16
$C_{60}H(OH)$	−5.75	−3.19	2.56	−122.22	C_s	32
C_{60}-O-C_{60}	−5.77	−3.31	2.46	−94.02	C_{2v}	32
$C_{60}H$-O-$C_{60}H$	−5.71	−3.27	2.44	−220.17	C_{2v}	32
$C_{59}N$	−4.58 (α spin) −5.94 (β spin)	−3.29 (α spin) −3.46 (β spin)	1.29 (α spin) 2.48 (β spin)	−	C_s	31
$C_{59}N(OH)$	−5.62	−3.24	2.38	−72.53	C_s	31
$(C_{59}N)_2$	−5.52	−3.29	2.23	−31.81	C_{2h}	31
$C_{59}N$-O-$C_{59}N$	−5.55	−3.33	2.22	−123.60	C_{2v}	31

The HOMOs and LUMOs of the ten molecular groups, calculated with B3LYP/6-311+G*, are presented in Figure S1, which are plotted with VESTA [47]. The isovalues for C_{60}-O-C_{60}, $C_{60}H$-O-$C_{60}H$, $(C_{59}N)_2$ and $C_{59}N$-O-$C_{59}N$ molecules were set to 0.02, while that of the other six molecular groups was set to 0.04. The calculated energy of HOMO and LUMO of C_{60}, $C_{59}N$ and $(C_{59}N)_2$ are in good agreement with the works of Mohammadi and colleagues [48–50]. It is notable that the two isomers of $C_{60}O$ had nearly the same energy gap and only a 2.11 kcal/mol difference in binding energy. Yet, they exhibit distinct electronic features, such as in O_3 adsorption [18].

2.1. Carbon K-edge NEXAFS and XES

The NEXAFS and XES spectra of carbon *K*-edges of the selected molecules, including the open [5,6] and closed [6,6] isomers of $C_{60}O$, $C_{60}H(OH)$, C_{60}-O-C_{60}, $C_{60}H$-O-$C_{60}H$, $C_{59}N(OH)$ and $C_{59}N$-O-$C_{59}N$, were plotted in Figure 2. The spectra of the C_{60}, $C_{59}N$, and $(C_{59}N)_2$ molecules were also plotted for comparison. Also, the experimental NEXAFS spectra of C_{60}, $[6,6]C_{60}O$ and $(C_{59}N)_2$ molecules we could find are reproduced from the work of Käämbre et al. [51] and Schulte et al. [52] for comparison, which are plotted in dashed lines. It is clear that simulated NEXAFS spectra of C_{60} and $[6,6]C_{60}O$ molecules are in good agreement with the experimental results. Our simulated spectra reproduced all the important characteristics of the experiment results.
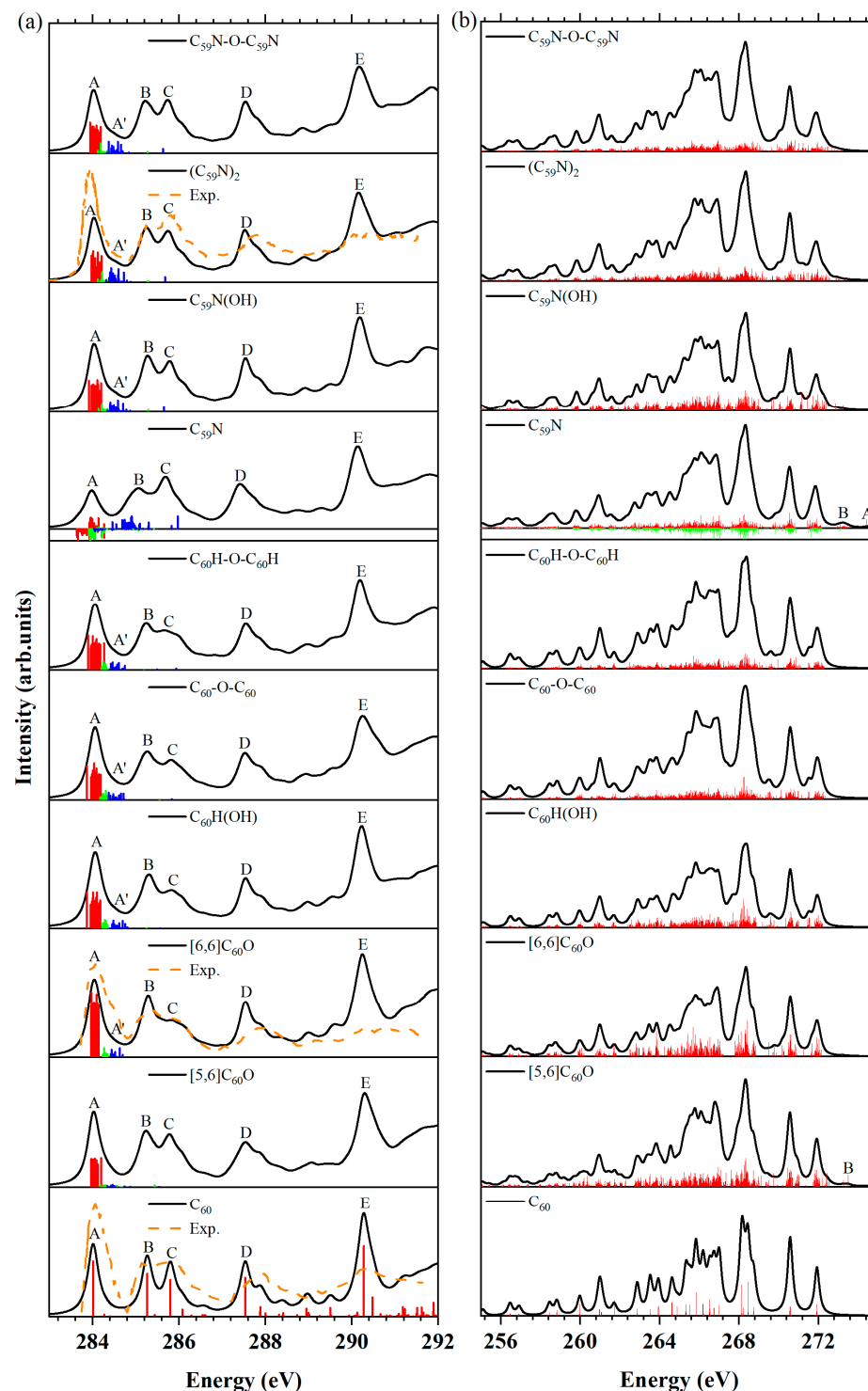
Figure 2. (**a**) NEXAFS spectra at the carbon *K*-edge of the fullerene C_{60}, aza[60]fullerene $C_{59}N$, their oxides and hydrates and $(C_{59}N)_2$. The orbital transitions from the $1s$ to the LUMO (shown as red bars), LUMO + 1 (shown as green bars) and LUMO + 2 (shown as blue bars) in the NEXAFS spectra of the nine molecules, along with the discrete intensities (shown as red bars) of the NEXAFS spectrum of the fullerene C_{60} molecule were plotted below each convoluted spectrum. For the $C_{59}N$ molecule, the contributions from β-spin electrons were marked as negative numbers. Experimental NEXAFS spectra of C_{60}, [6,6]C_{60}O [51] and $(C_{59}N)_2$ molecules [52] have been shifted −0.5 eV (shown as dashed lines). (**b**) Simulated XES spectra at the carbon *K*-edge of the fullerene C_{60}, aza[60]fullerene $C_{59}N$, their oxides and hydrates and $(C_{59}N)_2$. The discrete XES intensities of all molecules were depicted in the form of red bars (α-spin) and green bars (β-spin, represented as negative numbers) within the convoluted XES spectra.

Carbon *K*-edge NEXAFS. The NEXAFS spectra in Figure 2a exhibit five distinct peaks (labeled A–E) at nearly identical energy positions for each molecule, as illustrated in Figure 1. In addition, the orbital transitions from the 1*s* to the LUMO (shown as red bars), LUMO + 1 (shown as green bars) and LUMO + 2 (shown as blue bars) in the NEXAFS spectra of the nine molecules, along with the discrete intensities (shown as red bars) of the NEXAFS spectrum of the fullerene C_{60} molecule were plotted below each convoluted spectrum. For the $C_{59}N$ molecule, the contributions from β-spin electrons are represented as negative numbers. Although the NEXAFS spectra of these ten molecules exhibit similar peak positions, some notable differences can be observed. Specifically, depending on their lower symmetry—C_{2h} for $(C_{59}N)_2$, C_{2v} for closed [6,6] isomer of $C_{60}O$, C_{60}-O-C_{60}, $C_{60}H$-O-$C_{60}H$, $C_{59}N$-O-$C_{59}N$ and *Cs* for open [5,6] isomer of $C_{60}O$, $C_{60}H(OH)$ and $C_{59}N(OH)$, the NEXAFS spectra of these molecules exhibit a larger number of molecular orbital (MO) transitions from C 1*s* orbitals to unoccupied orbitals within each peak in comparison to that of C_{60}. From the feature peak E to their low-energy region, which corresponds to the C *K*-shell 1*s* absorption edges, signals that the C *K*-shell 1*s* absorption edges of all ten molecules are nearly identical. This indicated that both fullerene C_{60} and aza[60]fullerene $C_{59}N$ maintain the same valence state of carbon even after oxidation or exposure to water.

In the oxides and hydrates of fullerene C_{60}, the NEXAFS spectrum of the closed [6,6] isomer of $C_{60}O$ resembles that of the $C_{60}H(OH)$ and $C_{60}H$-O-$C_{60}H$, as they all have a relatively weak and broad peak C and a strong peak B, and a very weak feature peak A′ between the peaks A and B can be observed. While peak B of the NEXAFS spectra of the other two molecules open the [5,6] isomer of $C_{60}O$, and C_{60}-O-C_{60} exhibit a slightly higher intensity than peak C, the feature peak A′ only traced in the C_{60}-O-C_{60} molecule. The feature peak A′ primarily arose from the carbon 1*s* orbital to the LUMO + 2. Notably, the transition 1*s* → LUMO + 2 is notably weaker in the open [5,6] isomer of $C_{60}O$. The feature peak A′ is linked to the change of electronic structures of the C_{60} molecule upon its interaction with another atom or molecule.

It is evident that the NEXAFS spectra for $C_{59}N(OH)$, $(C_{59}N)_2$ and $C_{59}N$-O-$C_{59}N$ molecules all have a weak feature peak A′, which is the marker of the oxides or reactions involving H_2O of aza[60]fullerene $C_{59}N$. However, they exhibit significant differences in comparison to that of the $C_{59}N$ molecule, which lacks peak A′. Remarkably, nearly all carbon atoms exhibit similar NEXAFS spectral feature peaks A, B, C, D and E, regardless of any specific molecule. However, there is one notable exception, where feature peak A lacks contribution from the nearest carbon atoms (C_1, C_2, C_3, C_4, C_5 in Figure 1) neighboring the nitrogen and oxygen atoms. This distinction in feature peak A among the spectra of the neighbor of the nitrogen, oxygen and other carbon atoms could be attributed to their distinct local (chemical) environments.

Carbon *K*-edge XES. The XES spectra at the carbon *K*-edge of the ten molecules were plotted in Figure 2b. The discrete XES intensities of [5,6]$C_{60}O$ and $C_{59}N$ are shown in red bars (α-spin) and green bars (β-spin). These bars are superimposed on their convoluted XES spectra. The XES spectra of these ten molecules exhibit limited discernible differences in contrast to the NEXAFS spectra, except for specific peaks. The peak A in the $C_{59}N$ molecule can be attributed to the MO transition from the HOMO to the 1*s* orbital of carbon atom C_3 [46], and the peak B can be attributed to the transitions from the HOMO to the 1*s* orbitals of other carbon atoms. Similarly, peak B in the [5,6]$C_{60}O$ isomer primarily arises from the MO transitions between the HOMO and the 1*s* orbital of the carbon atoms. Consequently, it might be beneficial to utilize the feature peak B in the XES spectrum of the [5,6]$C_{60}O$ isomer to examine its presence within C_{60}. Although the experimental aspects might pose certain challenges, employing these distinctive features can provide valuable insights into their existence within the C_{60} crystalline and provide effective evidence for distinguishing the open [5,6] isomers of $C_{60}O$ from oxides and hydrates of C_{60}.

In summary, the carbon *K*-edge NEXAFS and XES spectra provide electronic structure information about the oxides and hydrates of C_{60} and $C_{59}N$, which can be used to distin-

guish the open [5,6] isomer of $C_{60}O$. However, distinguishing other oxides and hydrates using these spectra remains challenging.

2.2. Nitrogen K-edge NEXAFS and XES

To detect the presence of $C_{59}N(OH)$ and $C_{59}N$-O-$C_{59}N$, which are the oxides or hydrates of aza[60]fullerene $C_{59}N$, the nitrogen *K*-edge NEXAFS and XES spectra were simulated, as shown in Figure 3. The spectra of the $C_{59}N$ and $(C_{59}N)_2$ were also plotted for comparison. The experimental NEXAFS spectrum of $(C_{59}N)_2$ molecule is shown in dashed lines reproduced from the work of Schulte and colleagues [52]. It can be found that the simulated and experimental spectra are in good agreement.
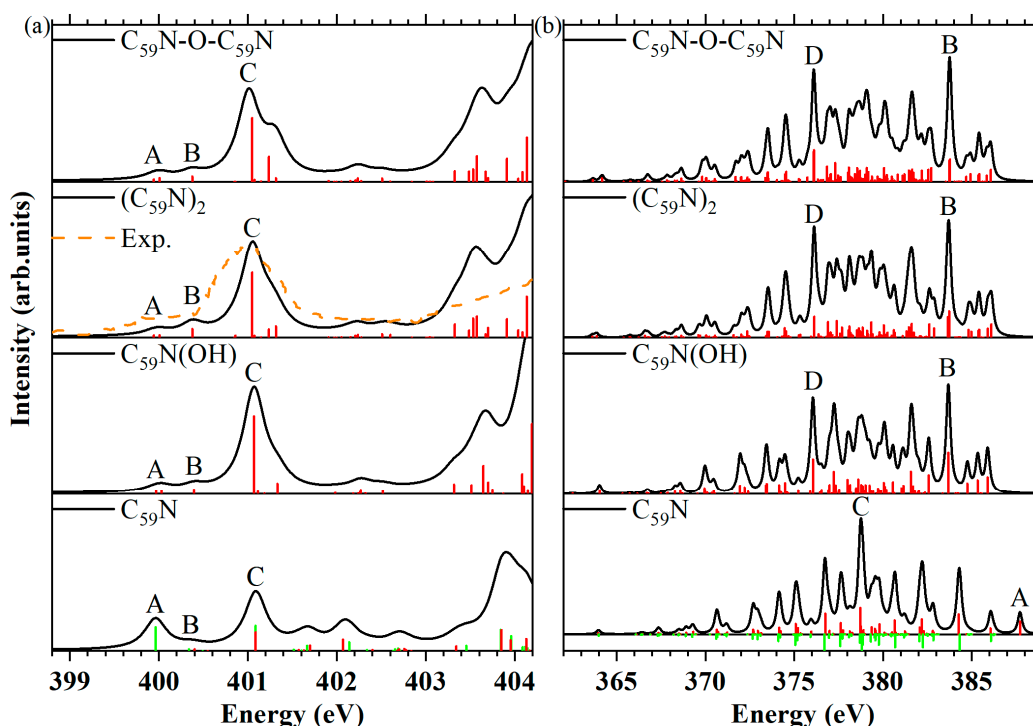
Figure 3. (**a**) Simulated NEXAFS spectra at the nitrogen *K*-edge of $C_{59}N$, $C_{59}N(OH)$, $(C_{59}N)_2$ and $C_{59}N$-O-$C_{59}N$ molecules, discrete intensities before convolution were represented by red bars for α-spin and green bars for β-spin. The experimental NEXAFS spectra of $(C_{59}N)_2$ molecule [52] are shown in dashed lines. (**b**) Simulated XES spectra at the nitrogen *K*-edge of these four molecules, discrete intensities of XES of all molecules were in red (α-spin) and green bars (β-spin, represented as negative numbers) within the convoluted XES spectra.

Nitrogen *K*-edge NEXAFS. Both the $C_{59}N(OH)$ and $C_{59}N$-O-$C_{59}N$ exhibit a faint shoulder A in the NEXAFS spectra (Figure 3a), which is attributed to the nitrogen 1*s* to LUMO transition. In contrast, the $C_{59}N$ molecule presents a relatively more pronounced first peak (peak A) at lower excitation energy, resulting from the nitrogen 1*s* → LUMO transition of β-spin. The MO transitions and corresponding energies of peak or shoulder A are available in Table S1. Despite the significance of the core-hole effect in comprehending NEXAFS spectra, the disparity observed in the nitrogen 1*s* → LUMO MO transition among the four molecules could be elucidated by considering the distribution of the LUMOs in the Ground state (GS). The LUMOs of $C_{59}N$(β-spin), $C_{59}N(OH)$, $(C_{59}N)_2$ and $C_{59}N$-O-$C_{59}N$ were plotted in Figure S1g–j, respectively. The LUMO of $C_{59}N$ exhibits a noticeable distribution around the nitrogen atom, whereas the LUMO of $C_{59}N(OH)$ exhibits a pronounced carbon character, similar to the $(C_{59}N)_2$, which fits well with prior results [53,54]. The LUMO in the $C_{59}N$-O-$C_{59}N$ molecule is predominantly concentrated on the intermolecular bond of carbon, which contributes to the existence of a weak shoulder A in their NEXAFS spectra.

Notably, the weak shoulder A observed in $C_{59}N(OH)$ and $C_{59}N-O-C_{59}N$ are valuable for distinguishing them from $C_{59}N$.

Nitrogen *K*-edge XES. The XES spectra at the nitrogen *K*-edge provide valuable insights, particularly when combining information obtained from GS calculations. In the case of the $C_{59}N(OH)$, $(C_{59}N)_2$ and $C_{59}N-O-C_{59}N$, their HOMOs exhibit some nitrogen characteristics, as illustrated in Figure S1h–j. For those compounds, the transitions from the HOMO to the nitrogen 1*s* orbital occur at relatively lower energies compared with the energy corresponding to the distinct peak A in the $C_{59}N$ molecule. The peak A in $C_{59}N$ originates from the transition from the HOMO (α-spin) to nitrogen 1*s* orbital transition [46]. Interestingly, the XES spectra of both $C_{59}N(OH)$ and $C_{59}N-O-C_{59}N$ exhibit strong and sharp feature peaks B and D, resembling those observed in $(C_{59}N)_2$. This similarity is in stark contrast to the sharp and pronounced feature, peak C, observed in the $C_{59}N$. These peaks are a result of transitions originating from deeper valence orbitals to the nitrogen 1*s* orbital(s), allowing for a clear distinction between $C_{59}N(OH)$ and $C_{59}N-O-C_{59}N$ when compared with $C_{59}N$.
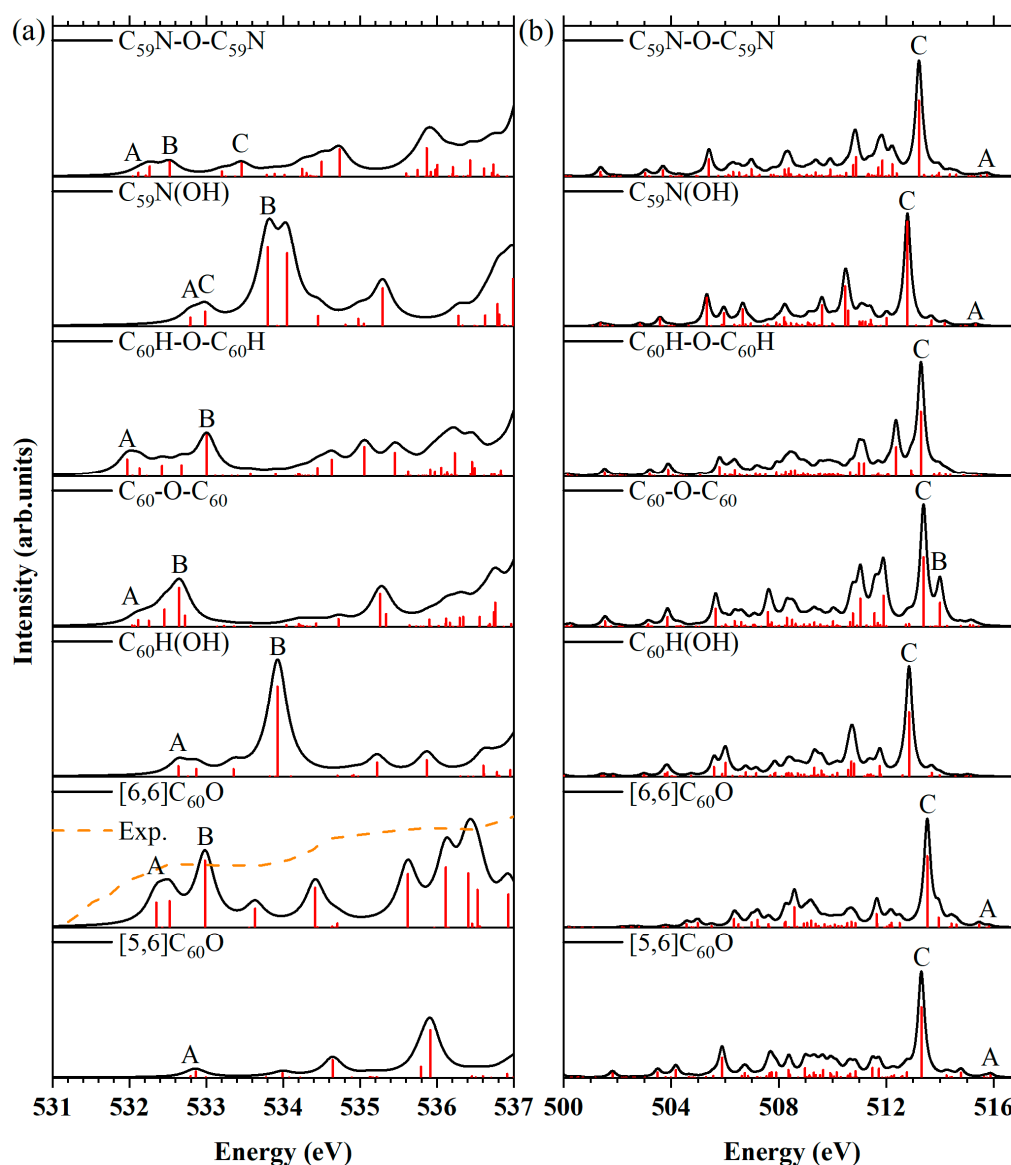
2.3. Oxygen K-edge NEXAFS and XES

Oxygen *K*-edge NEXAFS. The simulated NEXAFS spectra at the oxygen *K*-edge of the seven oxygen-containing molecules are shown in Figure 4a. The experimental NEXAFS spectrum of $[6,6]C_{60}O$ molecule is shown in the dashed line, which is reproduced from the work of Wohlers et al. at 370K [55]. The energy positions of peak (shoulder) A (corresponds to 1s → LUMO molecular orbital transition) and peaks B and C are listed in Table 2. Both the $[6,6]C_{60}O$ and the $C_{60}H-O-C_{60}H$ produce the first shoulder A or peak A with moderate intensity, which arises from the transition of oxygen 1*s* to the LUMO. The peak A of the NEXAFS spectra of the closed [6,6] isomer of $C_{60}O$ is observed at a higher excitation energy (532.35 eV), whereas it appears at a lower excitation energy in the $C_{60}H-O-C_{60}H$ (531.97 eV). Conversely, the oxygen 1*s* → LUMO transition only produces a weak peak A in the $C_{60}H(OH)$ and a weak shoulder A in the $[5,6]C_{60}O$, $C_{60}-O-C_{60}$, $C_{59}N(OH)$ and $C_{59}N-O-C_{59}N$ molecules. The disparity observed in the oxygen 1*s* → LUMO transition among these seven molecules could also be elucidated by examining the distribution of their LUMOs in the GS. Unlike the $[5,6]C_{60}O$, $C_{60}H(OH)$, $C_{60}-O-C_{60}$, $C_{59}N(OH)$ and $C_{59}N-O-C_{59}N$, whose LUMOs have strong carbon character (Figure S1b,d,e,h,j), the LUMOs of the $[6,6]C_{60}O$ and the $C_{60}H-O-C_{60}H$ molecules present here also exhibit some distribution around the oxygen atom (Figure S1c,f). Therefore, their NEXAFS spectra exhibit a moderate shoulder A or peak A. In particular, the moderately strong shoulder A with its relatively high excitation energy in the $[6,6]C_{60}O$ and the moderately strong peak A with its relatively low excitation energy in the $C_{60}H-O-C_{60}H$ can be considered as the fingerprint of their existence.

Table 2. Energy of peak (shoulder) A, peaks B and C in the O *K*-edge NEXAFS for the [5,6] and [6,6] isomers of $C_{60}O$, $C_{60}H(OH)$, $C_{60}-O-C_{60}$, $C_{60}H-O-C_{60}H$, $C_{59}N(OH)$ and $C_{59}N-O-C_{59}N$.

Molecule	Peak (Shoulder) A (eV) (1*s* → LUMO)	Peak B (eV)	Peak C (eV)
$[5,6]C_{60}O$	532.80	—	—
$[6,6]C_{60}O$	532.35	532.98	—
$C_{60}H(OH)$	532.64	533.93	—
$C_{60}-O-C_{60}$	532.03	532.64	—
$C_{60}H-O-C_{60}H$	531.97	533.00	—
$C_{59}N(OH)$	532.78	533.82	532.97
$C_{59}N-O-C_{59}N$	532.04	532.51	533.45

Figure 4. (**a**) Simulated NEXAFS spectra at the oxygen *K*-edge of the open [5,6] and closed [6,6] isomers of $C_{60}O$, $C_{60}H(OH)$, C_{60}-O-C_{60}, $C_{60}H$-O-$C_{60}H$, $C_{59}N(OH)$ and $C_{59}N$-O-$C_{59}N$, discrete intensities before convolution were in red bars. The experimental NEXAFS spectrum of [6,6]$C_{60}O$ molecule [55] is shown in dashed lines. (**b**) Simulated XES spectra at the oxygen *K*-edge of these seven oxygen-containing molecules, discrete intensities of XES of all molecules were in red bars within the convoluted XES spectra.

Furthermore, in the case of the [5,6]$C_{60}O$, $C_{60}H(OH)$ and $C_{59}N(OH)$, the oxygen $1s$ → LUMO transition is shown in the initial peak A or shoulder A with a weak intensity at nearly identical higher excitation energies (532.80 eV, 532.64 eV and 532.78 eV), among the five molecules with pronounced carbon characteristics in their LUMOs. The molecular groups, including the open [5,6] isomer of $C_{60}O$, $C_{60}H(OH)$ and $C_{59}N(OH)$, show that the absence of a strong peak B in comparison to the other two molecules, which can serve as the fingerprint of [5,6]$C_{60}O$. Additionally, $C_{60}H(OH)$ can be distinguished by the presence of a distinct peak B, while the presence of $C_{59}N(OH)$ can be recognized by the strong peak B and weak peak C. The spectra of the other two molecules, C_{60}-O-C_{60} and $C_{59}N$-O-$C_{59}N$, fall into another category, in which the oxygen $1s$ → LUMO transition generates the initial shoulder A with a weak intensity at nearly identical lower excitation energies (532.03 eV and 532.04 eV). These could be attributed to the influence of another carbon cage. At

the same time, the energy positions of their peak B are also quite similar (532.64 eV and 532.51 eV). Nevertheless, the distinct feature peak C at 533.45 eV in the $C_{59}N$-O-$C_{59}N$ molecule serves as its distinguishing characteristic compared with C_{60}-O-C_{60}.

Oxygen *K*-edge XES. The XES spectra at the oxygen *K*-edge are shown in Figure 4b. The MO transitions and corresponding energies of peak A are compared in Table S2. The XES spectrum of the [5,6] and [6,6] isomers of $C_{60}O$, as well as the $C_{59}N$-O-$C_{59}N$, exhibit a discernible weak peak A at high energy (515.88 eV, 515.82 eV and 515.74 eV). These peaks arise from the HOMO to oxygen 1s orbital transition. The HOMOs of the [5,6] and [6,6] isomers of $C_{60}O$ and $C_{59}N$-O-$C_{59}N$, as depicted in Figure S1b,c,j, exhibit some characteristics of oxygen. This results in the manifestation of the moderate peak A in their XES spectra. Conversely, the HOMOs of $C_{60}H(OH)$, C_{60}-O-C_{60} and $C_{60}H$-O-$C_{60}H$ possess strong carbon attributes, as shown in Figure S1d–f. The transition from the HOMO to the oxygen 1s orbital does not result in the observation of any discernible peaks in their XES spectra. For the $C_{59}N(OH)$, although its HOMOs also exhibit little oxygen characteristics, the transition from the HOMO to the oxygen 1s orbital occurs at relatively lower energy (515.33 eV) compared with the [5,6] and [6,6] isomers of $C_{60}O$, as well as $C_{59}N$-O-$C_{59}N$. Significantly, the XES spectra reveal distinct characteristics, including the moderately strong peak B in the C_{60}-O-C_{60}, as well as the uniformly strong and sharp peak C in all seven molecules. These peaks arise from transitions originating in the deeper valence orbitals to the oxygen 1s orbital, allowing for the distinction of oxides or hydrates of different fullerene and azafullerene.

2.4. XPS Shake-Up Satellites

Carbon *K*-edge XPS shake-up satellites. The calculated XPS shake-up satellites at the carbon *K*-edge for the fullerene C_{60}, aza[60]fullerene $C_{59}N$, their oxides and reactions involving H_2O and $(C_{59}N)_2$ were plotted in Figure 5a. Additionally, spectra of C_{60}, $C_{59}N$ and $(C_{59}N)_2$ were also provided for comparison. The XPS main lines of all symmetrically inequivalent carbon atoms are represented as red bars underneath each XPS shake-up spectrum of the other nine members. Contributions from the β-spin electrons in the $C_{59}N$ molecule were plotted as green bars. The experimental XPS shake-up satellite spectrum of $(C_{59}N)_2$ molecule is reproduced from the work of Schulte et al. [52], which is in agreement very well with our simulated spectrum. It is evident that the XPS shake-up satellites of the oxides or hydrates of fullerene C_{60} show significantly different profiles compared with those of C_{60}, except for that of [6,6] $C_{60}O$. This observation signifies an alteration in the electronic structures of the valence orbitals following the oxidation or reaction with water of the C_{60} molecule. Similarly, the spectra of the $C_{59}N(OH)$ and $C_{59}N$-O-$C_{59}N$ exhibit distinct profiles compared with those of the $C_{59}N$ and aza[60]fullerene dimer $(C_{59}N)_2$.

The spectra of these ten molecules exhibit very similar profiles, featuring prominent peaks A and C located proximate to the XPS main line, except for C_{60} and [6,6]$C_{60}O$. The presence of shoulder B can be attributed to contributions from several carbon atoms in $C_{60}H(OH)$. The primary contributions to the peaks A and C in the nine molecules have been elucidated and are collected in Table 3. It is interesting that except for the peak C in the open [5,6] isomer of $C_{60}O$, $C_{59}N$, $C_{59}N(OH)$ and $C_{59}N$-O-$C_{59}N$, resulting from the shake-up mechanisms, the primary contributions to the peaks A and C in the other five molecules are actually the XPS main lines of the atoms C_1, C_2, C_3, C_4 and C_5. It is evident that the carbon atom C_1 (sp^2-like) is connected to the oxygen atom, C_3 (in the $C_{59}N$) and C_5 (in the $C_{59}N$, $C_{59}N(OH)$, $(C_{59}N)_2$ and $C_{59}N$-O-$C_{59}N$) are bonded to the nitrogen atom with sp^2-like, while the carbon atoms C_2 (connected to the oxygen atom), C_3 (in the $C_{60}H(OH)$, C_{60}-O-C_{60}, $C_{60}H$-O-$C_{60}H$, $C_{59}N(OH)$, $(C_{59}N)_2$, and $C_{59}N$-O-$C_{59}N$) and C_4 (in the $C_{60}H(OH)$, C_{60}-O-C_{60}, and $C_{60}H$-O-$C_{60}H$) are sp^3-like atoms in the closed [6,6] isomer of $C_{60}O$, $C_{60}H(OH)$, C_{60}-O-C_{60}, $C_{60}H$-O-$C_{60}H$, $C_{59}N(OH)$, $(C_{59}N)_2$ and $C_{59}N$-O-$C_{59}N$ (Figure 1b–j). Hence, their binding energies exhibit a slight increase compared with those of other carbon atoms. The hybridization of carbon atoms and the blue-shifted binding energy of these hybridized

carbon atoms relative to the XPS main line for the oxides or hydrates of fullerene C_{60} and aza[60]fullerene $C_{59}N$ are collected in Table 4.
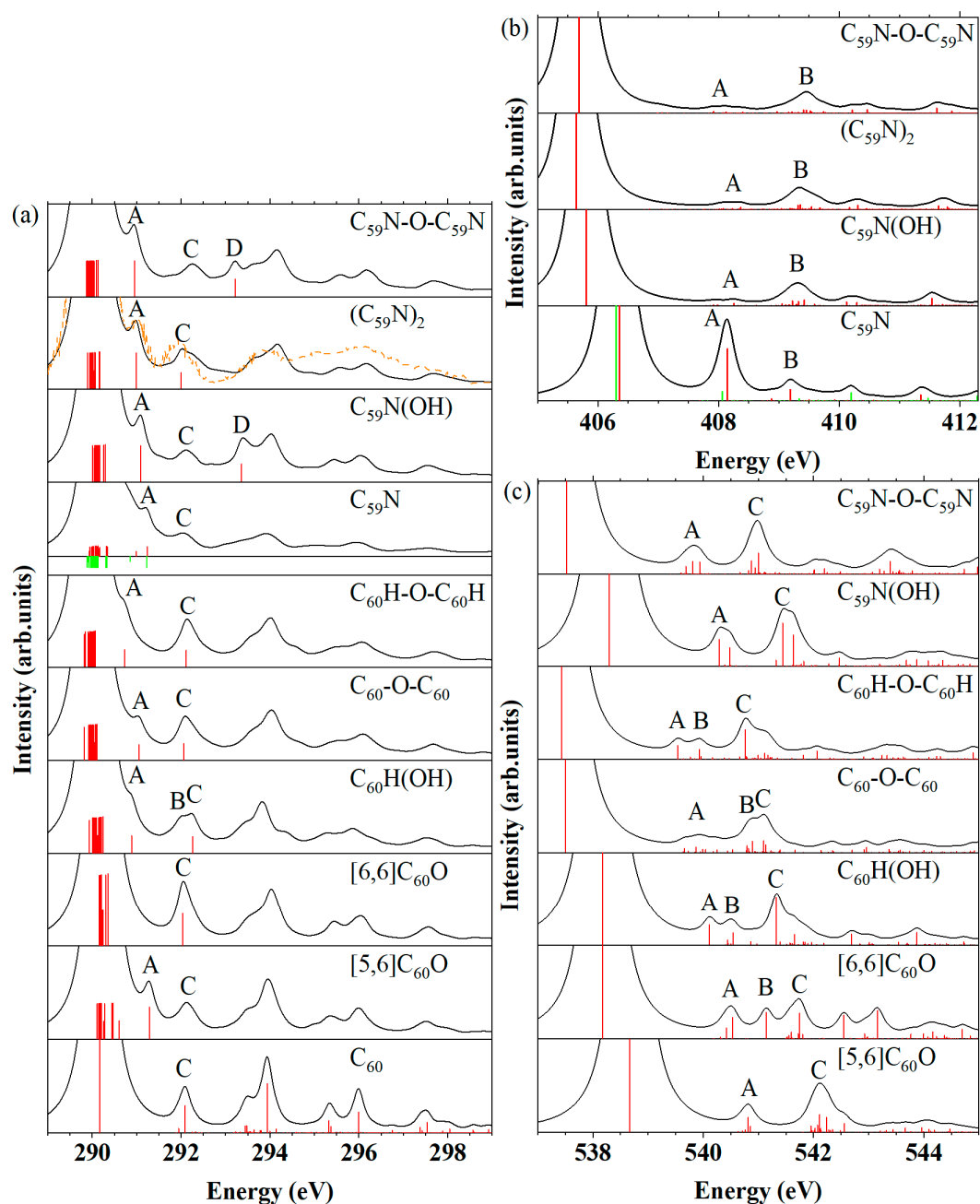
Figure 5. (**a**) XPS shake-up satellites at the carbon *K*-edge for the fullerene C_{60}, aza[60]fullerene $C_{59}N$, their oxides and hydrates and $(C_{59}N)_2$, along with the discrete intensities of the C_{60} molecule before convolution were depicted as red bars. The XPS main lines of all symmetrically inequivalent carbon atoms are represented as red bars underneath each XPS shake-up spectrum of the other nine members. Contributions from the β-spin electrons in the $C_{59}N$ molecule are shown as green bars. The experimental XPS shake-up satellite spectrum of $(C_{59}N)_2$ molecule [52] is shown as dashed lines. (**b**) XPS shake-up satellites at the nitrogen *K*-edge for $C_{59}N$, $C_{59}N(OH)$, $(C_{59}N)_2$ and $C_{59}N$-O-$C_{59}N$ molecules, along with the discrete intensities before convolution, are depicted as red bars. Contributions from the β-spin electrons are also shown as green bars under the spectrum in the $C_{59}N$ molecule. (**c**) XPS shake-up satellites at the oxygen *K*-edge for the open [5,6] and closed [6,6] isomers of $C_{60}O$, $C_{60}H(OH)$, C_{60}-O-C_{60}, $C_{60}H$-O-$C_{60}H$, $C_{59}N(OH)$ and $C_{59}N$-O-$C_{59}N$, along with the discrete intensities before convolution are shown as red bars.

Table 3. The C *K*-edge XPS shake-up satellites of the fullerene C_{60}, aza[60]fullerene $C_{59}N$, their oxides and hydrates.

Molecule	A	C
$[5,6]C_{60}O$	C_1: 291.284 eV	... [a]
$[6,6]C_{60}O$	-	C_2: 292.035 eV
$C_{60}H(OH)$	C_4: 290.888 eV	C_3: 292.257 eV
C_{60}-O-C_{60}	C_3: 291.055 eV	C_4: 292.064 eV
$C_{60}H$-O-$C_{60}H$	C_4: 290.735 eV	C_3: 292.114 eV
$C_{59}N$	C_5: 291.245 eV (α spin)	... [a]
	C_5: 291.228 eV (β spin)	
$C_{59}N(OH)$	C_5: 291.096 eV	... [a]
$(C_{59}N)_2$	C_5: 290.989 eV	C_3: 292.003 eV
$C_{59}N$-O-$C_{59}N$	C_5: 290.952 eV	... [a]

[a] XPS shake-up satellites originating from multiple carbon atoms.

Table 4. The hybridization of carbon atoms and the blue-shifted binding energy of these hybridized carbon atoms relative to the XPS main line in the oxides or hydrates of fullerene C_{60} and aza[60]fullerene $C_{59}N$.

Molecule	sp^2-like Carbon Atom (Blue-Shift)	sp^3-like Carbon Atom (Blue-Shift)
$[5,6]C_{60}O$	C_1 ($\sim$1 eV)	-
$[6,6]C_{60}O$	-	C_2 ($\sim$2 eV)
$C_{60}H(OH)$	-	C_3 ($\sim$2 eV)
	-	C_4 ($\sim$1 eV)
C_{60}-O-C_{60}	-	C_3 ($\sim$1 eV)
	-	C_4 ($\sim$2 eV)
$C_{60}H$-O-$C_{60}H$	-	C_3 ($\sim$2 eV)
	-	C_4 ($\sim$1 eV)
$C_{59}N$	C_3 (–)	-
	C_5 ($\sim$1 eV)	-
$C_{59}N(OH)$	C_5 ($\sim$1 eV)	C_3 ($\sim$3 eV)
$(C_{59}N)_2$	C_5 ($\sim$1 eV)	C_3 ($\sim$2 eV)
$C_{59}N$-O-$C_{59}N$	C_5 ($\sim$1 eV)	C_3 ($\sim$3 eV)

The local electronic structures of the C_3 and C_4 atoms in the oxides or hydrates of fullerene C_{60} show minimal changes after bonding with other atoms (like H atom), such as (C_4 in the $C_{60}H(OH)$ and C_4 in the $C_{60}H$-O-$C_{60}H$), or a large molecule (like C_3 in the C_{60}-O-C_{60}), although they become an sp^3-like carbon, and consequently lead to blue-shifted binding energy—around 1 eV in the $C_{60}H(OH)$ (C_4), C_{60}-O-C_{60} (C_3) and $C_{60}H$-O-$C_{60}H$ (C_4) in comparison to their XPS main line. In contrast, sp^3-like carbon atoms bonded to oxygen atoms are shown a pronounced blue-shifted in their binding energy—approximately 2 eV in the closed [6,6] isomer of $C_{60}O(C_2)$, $C_{60}H(OH)$ (C_3), C_{60}-O-C_{60} (C_4) and $C_{60}H$-O-$C_{60}H$ (C_3) when compared with their XPS main line. The larger blue shifts demonstrated the local electronic structures of the sp^3-like C_2, C_3 and C_4 atoms changing a lot after being connected to an oxygen atom (such as C_2 in the $[6,6]C_{60}O$, C_3 in the $C_{60}H(OH)$ and $C_{60}H$-O-$C_{60}H$, C_4 in the C_{60}-O-C_{60}). The C *K*-edge XPS shake-up satellite spectra reveal the distinctive features of the $[6,6]C_{60}O$ molecule, characterized by a strong peak C and the absence of peak A, while $C_{60}H(OH)$ exhibits a unique shoulder B in its spectrum. Therefore, C *K*-edge XPS shake-up satellites serve as a valuable technique for detecting the presence of $[6,6]C_{60}O$ and $C_{60}H(OH)$ molecules, enabling their differentiation from other fullerene C_{60} oxides and hydrates.

In the oxides or hydrates of azafullerene $C_{59}N$, the binding energy of carbon atom C_5 is blue-shifted by approximately 1 eV relative to the XPS main line, while the binding energy of carbon atom C_3 remains unchanged in the $C_{59}N$ molecule [46]. However, upon oxidation (e.g., $C_{59}N$-O-$C_{59}N$) or reaction with water (e.g., $C_{59}N(OH)$), the local electronic structure of

the carbon atom C_3 undergoes significant alteration, transforming it into a *sp^3*-like carbon atom in the $C_{59}N(OH)$ and $C_{59}N$-O-$C_{59}N$. Consequently, a substantial blue-shift binding energy of around 3 eV is observed in the $C_{59}N(OH)$ and $C_{59}N$-O-$C_{59}N$ compared to their XPS main line, while the blue-shift is approximately 2 eV in the $(C_{59}N)_2$[46]. The unique peak D in the spectra of $C_{59}N(OH)$ and $C_{59}N$-O-$C_{59}N$ molecules distinguish them from $C_{59}N$ and $(C_{59}N)_2$ molecules. However, the C *K*-edge XPS shake-up satellite spectra could not differentiate between $C_{59}N(OH)$ and $C_{59}N$-O-$C_{59}N$ molecules.

It is noteworthy that only C_1 exhibits a *sp^2*-like hybridization, leading to a subtle blue shift in binding energy relative to the XPS main line among all the carbon atoms bonded to an oxygen atom. The uniqueness of the C_1 atom demonstrates a remarkable change in the localized electronic structure of C_1 in the [5,6]$C_{60}O$ isomer after breaking the five- and six-membered ring structures of the fullerene cage.

Nitrogen *K*-edge XPS shake-up satellites. The alterations in electronic structures can be elucidated through the analysis of nitrogen *K*-edge XPS shake-up satellites (Figure 5b). The energy of peak B in the spectra for the $C_{59}N$, $C_{59}N(OH)$, $(C_{59}N)_2$ and $C_{59}N$-O-$C_{59}N$ are shown in Table 5. In both $C_{59}N(OH)$ and $C_{59}N$-O-$C_{59}N$, peak A is relatively weaker compared with that of the $C_{59}N$. Furthermore, peak B in $C_{59}N$-O-$C_{59}N$ exhibits a blue shift of approximately 0.15 eV compared with peak B of the $C_{59}N(OH)$. An extensive assignment of the principal contributions to peaks A and B, which are observed in the nitrogen *K*-edge XPS shake-up satellites of these four members within the $C_{59}N$ family, is provided in Table S3. The information can serve as a valuable reference for future experimental investigations. It is evident that, apart from $C_{59}N$ and $C_{59}N(OH)$, feature B in the other two molecules is attributed to excitations originating from deeper valence orbitals.

Table 5. Energy of peak B in the N *K*-edge XPS shake-up satellites for the $C_{59}N$, $C_{59}N(OH)$, $(C_{59}N)_2$ and $C_{59}N$-O-$C_{59}N$ molecules.

Molecule	Energy of Peak B (eV)
$C_{59}N$	409.19
$C_{59}N(OH)$	409.31
$(C_{59}N)_2$	409.34
$C_{59}N$-O-$C_{59}N$	409.46

Oxygen *K*-edge XPS shake-up satellites. The alterations in electronic structures can also be discerned from the oxygen *K*-edge XPS shake-up satellites, as depicted in Figure 5c. The energies of peaks A, B and C in the oxygen *K*-edge XPS shake-up satellites are shown in Table 6 for the seven oxygen-containing molecules. The [6,6]$C_{60}O$, $C_{60}H(OH)$, C_{60}-O-C_{60} and $C_{60}H$-O-$C_{60}H$ exhibit three feature peaks A, B and C. The other three molecules, open [5,6] isomer of $C_{60}O$, $C_{59}N(OH)$ and $C_{59}N$-O-$C_{59}N$, do not show a discernible peak B, highlighting a noticeable difference between the [6,6]$C_{60}O$, $C_{60}H(OH)$, C_{60}-O-C_{60} and $C_{60}H$-O-$C_{60}H$. In comparison to the [5,6]$C_{60}O$ molecule, the featured peak A of $C_{59}N(OH)$ demonstrates a red shift of 0.52 eV, whereas the characteristic peak A of the $C_{59}N$-O-$C_{59}N$ exhibits a red shift of 1.00 eV. In contrast, in comparison with [6,6]$C_{60}O$, the characteristic peak A of $C_{60}H(OH)$ shows a red shift of 0.42 eV, the feature peak A of the C_{60}-O-C_{60} exhibits a red shift of 0.66 eV, and the characteristic peak A of the $C_{60}H$-O-$C_{60}H$ shows a red shift of 1.00 eV. Hence, the oxygen *K*-edge XPS shake-up satellites offer a valuable technique to detect the presence of these seven molecules, which can also be used to distinguish them from other oxides or hydrates family members of fullerene C_{60} and aza[60]fullerene $C_{59}N$.

The detailed assignments of the primary contributions to peaks A, B and C within the oxygen *K*-edge XPS shake-up satellites for these seven oxygen-containing molecules are collected in Table S4, which can provide a valuable reference for future experiments. It is notable that peak B includes excitations from deeper valence orbitals in C_{60}-O-C_{60}. With the exception of $C_{60}H(OH)$ and $C_{59}N(OH)$ molecules, peak C also encompasses excitations from deeper valence orbitals in the remaining five molecules.

Table 6. Energy of peaks A, B and C in the O *K*-edge XPS shake-up satellites for the [5,6] and [6,6] isomers of $C_{60}O$, $C_{60}H(OH)$, C_{60}-O-C_{60}, $C_{60}H$-O-$C_{60}H$, $C_{59}N(OH)$ and $C_{59}N$-O-$C_{59}N$.

Molecule	Energy of Peak A (eV)	Energy of Peak (Shoulder) B (eV)	Energy of Peak C (eV)
[5,6]$C_{60}O$	540.81	-	542.11
[6,6]$C_{60}O$	540.53	541.14	541.75
$C_{60}H(OH)$	540.11	540.54	541.33
C_{60}-O-C_{60}	539.87	540.89	541.10
$C_{60}H$-O-$C_{60}H$	539.53	539.94	540.76
$C_{59}N(OH)$	540.29	-	541.44
$C_{59}N$-O-$C_{59}N$	539.81	-	541.00

3. Computational Details

The ten groups of molecular models are presented in Figure 1, including fullerene(C_{60}), $C_{60}O$ with oxygen in the [5,6] open annulene and [6,6] closed epoxide isomers, $C_{60}H(OH)$, ether-oxygen-bridged fullerene dimer C_{60}-O-C_{60}, $C_{60}H$-O-$C_{60}H$, aza[60]fullerene $C_{59}N$, $C_{59}N(OH)$, $(C_{59}N)_2$ and $C_{59}N$-O-$C_{59}N$, in which C_{60}, $C_{59}N$ and $(C_{59}N)_2$ molecules are used for comparison. All the molecular configurations were optimized, and the single point energy calculations were performed with the Gaussian16 program at the B3LYP/6-31G(d,p) level [56], and the optimized configurations were subsequently validated as energy minima through frequency calculations. All structures were optimized without initial symmetry constraints. The geometries with Cartesian coordinates of all optimized structures are listed in Table S7 The lowest frequencies of these structures are collected in Table S5, while the energies of the ten molecules with different spin multiplicities are collected in Table S6. The electronic state with the lowest energy was applied for the soft X-ray spectra simulations. Nitrogen, oxygen and their attached carbon atoms are shown in Figure 1b–j, where atoms C_1 and C_1', C_2 and C_2', C_3 and C_3', C_4 and C_4' and C_5 and C_5' are symmetrically equivalent atoms.

The $Z + 1$ approximation and TP method have been employed for the efficient computation of large systems [57–59], which are characterized by a high number of MOs in the NEXAFS and XES spectroscopy calculations. To ensure computing precision, the FCH potential method was adopted for the accurate characterization of NEXAFS spectra [60–64]. The triple-ζ quality individual gauge for localized orbital (IGLO-III) basis set was selected for the excited carbon, nitrogen or oxygen atoms, while other non-excited atoms were calculated by employing model core potentials (MCP), which was defined as the Huzinaga's procedure [65] implemented in the StoBe program [66–68]. This computing strategy ensured the accuracy and speed for large-scale computing in our soft X-ray spectroscopy calculations [60,61]. Additionally, to enhance the accuracy, an augmented diffuse basis set (19s, 19p and 19d) for the excited carbon, nitrogen or oxygen atoms was utilized in the NEXAFS spectra calculations.

The NEXAFS spectra and ΔKohn–Sham (ΔKS) [60] calculations were carried out using StoBe [66–68]. The relativistic effects were accounted for by introducing energy shifts of +0.2 eV for the carbon *K*-edge, +0.3 eV for the nitrogen *K*-edge and +0.5 eV for the oxygen *K*-edge [69]. The NEXAFS spectra were generated by convoluting discrete intensities with a Lorentzian function, which incorporated spectral broadening. For energies below the ionization potential (IP), the full width at half maximum (FWHM) was set to 0.3 eV. In the range from the IP to 5 eV above, the FWHM increased linearly up to 1.0 eV. For energies beyond that range, a constant FWHM of 1.0 eV was employed. The XES spectra were simulated employing the BioNano-LEGO developed by Yi Luo's group [70]. GS wave functions were derived from the Gaussian16 program [56] at the B3LYP/6-311+G* level. The computed XES spectra underwent additional convolution with a Lorentzian function, employing an FWHM of 0.3 eV.

The ECH-KS method was employed for XPS shake-up satellite spectra calculations [71–73], which has been introduced for the calculation of the numerous excited states necessary for the XPS shake-up satellites in large systems [74]. The 6-31G basis set was applied to the non-ionized

atoms, while the IGLO-III basis set was utilized for the core-ionized carbon, nitrogen or oxygen atom [75]. The shake-up satellites were calculated by the ECH-KS method, which was consistent with ECH-TDDFT calculations and experimental results, as previously validated [75–77]. In our calculations, the XPS shake-up satellites were also performed by BioNano-LEGO [70]. The shake-up intensities were convolved with a Lorentzian function with an FWHM of 0.3 eV.

4. Conclusions

The core-hole excitation spectroscopic techniques, specifically NEXAFS, XES and XPS shake-up satellites, were employed to differentiate between various members of the oxides or hydrates family members of fullerene C_{60} and aza[60]fullerene $C_{59}N$. These members include the open [5,6] and closed [6,6] isomers of $C_{60}O$, $C_{60}H(OH)$, C_{60}-O-C_{60}, $C_{60}H$-O-$C_{60}H$, $C_{59}N(OH)$ and $C_{59}N$-O-$C_{59}N$. These spectra provided us with comprehensive insights into both the unoccupied and occupied molecular orbitals of the molecular groups under study. Meanwhile, the oxygen *K*-edge NEXAFS, carbon and oxygen *K*-edge XPS shake-up satellite spectra were employed to distinguish oxides or hydrates of fullerene C_{60} and azafullerene $C_{59}N$. The approach allowed us to delve deeply insights into the relationships between individual spectral peaks and the electronic and geometric structures of the molecules within the fullerene C_{60} and aza[60]fullerene $C_{59}N$ families. These findings not only enhance our understanding of these complex molecular systems but also pave the way for future research and applications in the field of nanomaterial science.

References

1. Nam, S.; Khim, D.; Martinez, G.T.; Varambhia, A.; Nellist, P.D.; Kim, Y.; Anthopoulos, T.D.; Bradley, D.D. Significant Performance Improvement in n-Channel Organic Field-Effect Transistors with C_{60}:C_{70} Co-Crystals Induced by Poly (2-ethyl-2-oxazoline) Nanodots. *Adv. Mater.* **2021**, *33*, 2100421. [CrossRef] [PubMed]
2. Benatto, L.; Marchiori, C.; Talka, T.; Aramini, M.; Yamamoto, N.; Huotari, S.; Roman, L.; Koehler, M. Comparing C_{60} and C_{70} as acceptor in organic solar cells: Influence of the electronic structure and aggregation size on the photovoltaic characteristics. *Thin Solid Films* **2020**, *697*, 137827. [CrossRef]
3. Alipour, E.; Alimohammady, F.; Yumashev, A.; Maseleno, A. Fullerene C_{60} containing porphyrin-like metal center as drug delivery system for ibuprofen drug. *J. Mol. Model.* **2020**, *26*, 7. [CrossRef]
4. Hong, I.-H.; Gao, C.-J.; Lin, K.-B.; Kaun, C.-C. Self-organized C_{70}/C_{60} heterojunction nanowire arrays on Si(110) for Si-based molecular negative differential resistance nanodevices. *Appl. Surf. Sci.* **2020**, *531*, 147338. [CrossRef]
5. Chen, L.; Wang, X.; Kumar, S. Thermal transport in fullerene derivatives using molecular dynamics simulations. *Sci. Rep.* **2015**, *5*, 12763. [CrossRef] [PubMed]
6. Socol, M.; Preda, N.; Costas, A.; Borca, B.; Popescu-Pelin, G.; Mihailescu, A.; Socol, G.; Stanculescu, A. Thin films based on cobalt phthalocyanine: C_{60} fullerene: ZnO hybrid nanocomposite obtained by laser evaporation. *Nanomaterials* **2020**, *10*, 468. [CrossRef]
7. Tanuma, Y.; Knaflič, T.; Anézo, B.; Stangel, C.; Volkmann, J.; Tagmatarchis, N.; Wegner, H.A.; Arčon, D.; Ewels, C.P. Long Spin Coherence Times on C_{59}N-C_{60} Heterodimer Radicals Entrapped in Cycloparaphenylene Rings. *J. Phys. Chem. C* **2023**, *127*, 6552–6561. [CrossRef]
8. Martín-Gomis, L.; Rotas, G.; Ohkubo, K.; Fernández-Lázaro, F.; Fukuzumi, S.; Tagmatarchis, N.; Sastre-Santos, Á. Does a nitrogen matter? Synthesis and photoinduced electron transfer of perylenediimide donors covalently linked to C_{59}N and C_{60} acceptors. *Nanoscale* **2015**, *7*, 7437–7444. [CrossRef]
9. Rotas, G.; Stranius, K.; Tkachenko, N.; Tagmatarchis, N. Ultralong 20 Milliseconds Charge Separation Lifetime for Photoilluminated Oligophenylenevinylene-Azafullerene Systems. *Adv. Funct. Mater.* **2018**, *28*, 1702278. [CrossRef]
10. Yin, H.; Lin, H.; Zong, Y.; Wang, X.-D. The recent advances in C_{60} micro/nanostructures and their optoelectronic applications. *Org. Electron.* **2021**, *93*, 106142. [CrossRef]
11. Kianezhad, M.; Youzi, M.; Vaezi, M.; Nejat Pishkenari, H. Unidirectional motion of C_{60}-based nanovehicles using hybrid substrates with temperature gradient. *Sci. Rep.* **2023**, *13*, 1100. [CrossRef]
12. Vinnikov, N.; Dolbin, A.; Basnukaeva, R.; Gavrilko, V.; Eselson, V.; Buravtseva, L. Quantum effects in the low-temperature thermal expansion of fullerite C_{60} doped with a 4He impurity. *Low Temp. Phys.* **2022**, *48*, 791–797. [CrossRef]
13. Elistratova, M.; Zakharova, I. Temperature-dependent photoluminescence of thin tetraphenylporphyrin-based thin films and their composites with C_{60} fullerene. *J. Mater. Sci. Mater. Electron.* **2022**, *33*, 15554–15562. [CrossRef]
14. Sivkov, D.V.; Petrova, O.V.; Nekipelov, S.V.; Vinogradov, A.S.; Skandakov, R.N.; Bakina, K.A.; Isaenko, S.I.; Ob'edkov, A.M.; Kaverin, B.S.; Vilkov, I.V.; et al. Quantitative Characterization of Oxygen-Containing Groups on the Surface of Carbon Materials: XPS and NEXAFS Study. *Appl. Sci.* **2022**, *12*, 7744. [CrossRef]
15. Lin, I.H.; Lu, Y.H.; Chen, H.T. Nitrogen-doped C_{60} as a robust catalyst for CO oxidation. *J. Comput. Chem.* **2017**, *38*, 2041–2046. [CrossRef]
16. Tang, K.; Chen, X.; Ding, X.; Yu, X.; Yu, X. MoS2/graphene oxide/C_{60}-OH nanostructures deposited on a quartz crystal microbalance transducer for humidity sensing. *ACS Appl. Nano Mater.* **2021**, *4*, 10810–10818. [CrossRef]
17. Esrafili, M.D.; Janebi, H. B-, N-doped and BN codoped C_{60} heterofullerenes for environmental monitoring of NO and NO$_2$: A DFT study. *Mol. Phys.* **2020**, *118*, e1631495. [CrossRef]
18. Tabari, L.; Farmanzadeh, D. Interesting adsorption behavior of C_{60}O fullerene oxide isomers toward O$_3$ and CO molecules: A DFT study. *Appl. Surf. Sci.* **2019**, *479*, 569–575. [CrossRef]
19. Dattani, R.; Gibson, K.F.; Few, S.; Borg, A.J.; DiMaggio, P.A.; Nelson, J.; Kazarian, S.G.; Cabral, J.T. Fullerene oxidation and clustering in solution induced by light. *J. Colloid Interface Sci.* **2015**, *446*, 24–30. [CrossRef] [PubMed]
20. Sanchís, J.; Freixa, A.; López-Doval, J.C.; Santos, L.H.; Sabater, S.; Barceló, D.; Abad, E.; Farré, M. Bioconcentration and bioaccumulation of C_{60} fullerene and C_{60} epoxide in biofilms and freshwater snails (*Radix* sp.). *Environ. Res.* **2020**, *180*, 108715. [CrossRef] [PubMed]
21. Jones, M.A.; Britz, D.A.; Morton, J.J.; Khlobystov, A.N.; Porfyrakis, K.; Ardavan, A.; Briggs, G.A.D. Synthesis and reactivity of N@C_{60}O. *Phys. Chem. Chem. Phys.* **2006**, *8*, 2083–2088. [CrossRef]
22. Mondal, T.; Tripathi, A.; Tiwari, A.; Zhang, J.; Shripathi, T.; Shinohara, H.J.J.o.A.P. Temperature and pressure induced Raman studies of C_{60} oxide. *J. Appl. Phys.* **2018**, *124*, 195105. [CrossRef]
23. Gao, B.; Chen, G. CO oxidization catalyzed by B, N, and their co-doped fullerenes: A first-principles investigation. *RSC. Adv.* **2019**, *9*, 21626–21636. [CrossRef]
24. Palotás, J.; Martens, J.; Berden, G.; Oomens, J. Laboratory IR Spectra of the Ionic Oxidized Fullerenes C_{60}O$^+$ and C_{60}OH$^+$. *J. Phys. Chem. A* **2022**, *126*, 2928–2935. [CrossRef] [PubMed]
25. Schulz, P.; Kelly, L.L.; Winget, P.; Li, H.; Kim, H.; Ndione, P.F.; Sigdel, A.K.; Berry, J.J.; Graham, S.; Brédas, J.L.; et al. Tailoring Electron-Transfer Barriers for Zinc Oxide/C_{60} Fullerene Interfaces. *Adv. Funct. Mater.* **2014**, *24*, 7381–7389. [CrossRef]
26. Tanaka, Y.; Kanai, K.; Ouchi, Y.; Seki, K. Oxygen effect on the interfacial electronic structure of C_{60} film studied by ultraviolet photoelectron spectroscopy. *Chem. Phys. Lett.* **2007**, *441*, 63–67. [CrossRef]

27. Wang, X.-B.; Woo, H.-K.; Kiran, B.; Wang, L.-S. Photoelectron Spectroscopy and Electronic Structures of Fullerene Oxides: $C_{60}O_x^-$ (x = 1–3). *J. Phys. Chem. A* **2005**, *109*, 11089–11092. [CrossRef] [PubMed]

28. Lim, J.; Park, J.; Yeom, G.Y. Interfacial electronic structure of molybdenum oxide on the fullerene layer, a potential hole-injecting layer in inverted top-emitting organic light-emitting diodes. *Curr. Appl. Phys.* **2013**, *13*, 1037–1041. [CrossRef]

29. Pan, F.; Ni, K.; Xu, T.; Chen, H.; Wang, Y.; Gong, K.; Liu, C.; Li, X.; Lin, M.-L.; Li, S.; et al. Long-range ordered porous carbons produced from C_{60}. *Nature* **2023**, *614*, 95–101. [CrossRef]

30. Tropin, T.V.; Karpets, M.L.; Kosiachkin, Y.; Gapon, I.V.; Gorshkova, Y.E.; Aksenov, V.L. Evaluation of fullerenes C_{60}/C_{70} layers in polystyrene thin films by neutron and X-ray reflectometry. *Fuller. Nanotub. Carbon Nanostructures* **2021**, *29*, 819–824. [CrossRef]

31. Asad, K.; Stergiou, A.; Kourtellaris, A.; Tagmatarchis, N.; Chronakis, N. First Synthesis of the Inherently Chiral Trans-4' Bisadduct of $C_{59}N$ Azafullerene by Using Cyclo-[2]-dodecylmalonate as a Tether. *Chem. Eur. J.* **2021**, *27*, 13879–13886. [CrossRef]

32. Couto, R.C.; Kjellsson, L.; Ågren, H.; Carravetta, V.; Sorensen, S.L.; Kubin, M.; Bülow, C.; Timm, M.; Zamudio-Bayer, V.; von Issendorff, B.; et al. The carbon and oxygen K-edge NEXAFS spectra of CO^+. *Phys. Chem. Chem. Phys.* **2020**, *22*, 16215–16223. [CrossRef]

33. de Kock, S.; Skudler, K.; Matsidik, R.; Sommer, M.; Müller, M.; Walter, M. NEXAFS spectra of model sulfide chains: Implications for sulfur networks obtained from inverse vulcanization. *Phys. Chem. Chem. Phys.* **2023**, *25*, 20395–20404. [CrossRef] [PubMed]

34. Wasowicz, T.; Ljubić, I.; Kivimäki, A.; Richter, R. Core–shell excitation of isoxazole at the C, N, and O K-edges–an experimental NEXAFS and theoretical TD-DFT study. *Phys. Chem. Chem. Phys.* **2022**, *24*, 19302–19313. [CrossRef] [PubMed]

35. Cole, J.; Henderson, Z.; Thomas, A.G.; Compeán-González, C.L.; Greer, A.J.; Hardacre, C.; Venturini, F.; Garzon, W.Q.; Ferrer, P.; Grinter, D.C.; et al. Near-ambient pressure XPS and NEXAFS study of a superbasic ionic liquid with CO_2. *J. Phys. Chem. C* **2021**, *125*, 22778–22785. [CrossRef]

36. Braglia, L.; Tavani, F.; Mauri, S.; Edla, R.; Krizmancic, D.; Tofoni, A.; Colombo, V.; D'angelo, P.; Torelli, P. Catching the Reversible Formation and Reactivity of Surface Defective Sites in Metal–Organic Frameworks: An Operando Ambient Pressure-NEXAFS Investigation. *J. Phys. Chem. Lett.* **2021**, *12*, 9182–9187. [CrossRef] [PubMed]

37. Johnson, M.; Hawly, T.; Zhao, B.; Halik, M.; Nefedov, A.; Fink, R. Field-induced modification of the electronic structure in BTBT-based organic thin films observed by NEXAFS spectroscopy. *Appl. Phys. Lett.* **2022**, *121*, 183503. [CrossRef]

38. Couto, R.C.; Hua, W.; Lindblad, R.; Kjellsson, L.; Sorensen, S.L.; Kubin, M.; Bülow, C.; Timm, M.; Zamudio-Bayer, V.; von Issendorff, B.; et al. Breaking inversion symmetry by protonation: Experimental and theoretical NEXAFS study of the diazynium ion, N_2H^+. *Phys. Chem. Chem. Phys.* **2021**, *23*, 17166–17176. [CrossRef] [PubMed]

39. Lever, F.; Mayer, D.; Metje, J.; Alisauskas, S.; Calegari, F.; Düsterer, S.; Feifel, R.; Niebuhr, M.; Manschwetus, B.; Kuhlmann, M.; et al. Core-level spectroscopy of 2-thiouracil at the sulfur L_1-and $L_{2,3}$-edges utilizing a SASE free-electron laser. *Molecules* **2021**, *26*, 6469. [CrossRef] [PubMed]

40. Klein, B.P.; Hall, S.J.; Maurer, R.J. The nuts and bolts of core-hole constrained ab initio simulation for K-shell x-ray photoemission and absorption spectra. *J. Phys. Condens. Matter* **2021**, *33*, 154005. [CrossRef]

41. Armillotta, F.; Bidoggia, D.; Biasin, P.; Annese, A.; Cossaro, A.; Verdini, A.; Floreano, L.; Peressi, M.; Vesselli, E. Spectroscopic fingerprints of iron-coordinated cobalt and iron porphyrin layers on graphene. *Cell Rep. Phys. Sci.* **2023**, *4*, 101378. [CrossRef]

42. Creegan, K.M.; Robbins, J.L.; Robbins, W.K.; Millar, J.M.; Sherwood, R.D.; Tindall, P.J.; Cox, D.M.; McCauley, J.P.; Jones, D.R. Synthesis and characterization of $C_{60}O$, the first fullerene epoxide. *J. Am. Chem. Soc.* **1992**, *114*, 1103–1105. [CrossRef]

43. Lebedkin, S.; Ballenweg, S.; Gross, J.; Taylor, R.; Krätschmer, W. Synthesis of $C_{120}O$: A new dimeric [60] fullerene derivative. *Tetrahedron Lett.* **1995**, *36*, 4971–4974. [CrossRef]

44. Weisman, R.B.; Heymann, D.; Bachilo, S.M. Synthesis and characterization of the "missing" oxide of C_{60}:[5,6]-open $C_{60}O$. *J. Am. Chem. Soc.* **2001**, *123*, 9720–9721. [CrossRef] [PubMed]

45. Erbahar, D.; Susi, T.; Rocquefelte, X.; Bittencourt, C.; Scardamaglia, M.; Blaha, P.; Guttmann, P.; Rotas, G.; Tagmatarchis, N.; Zhu, X.; et al. Spectromicroscopy of C_{60} and azafullerene $C_{59}N$: Identifying surface adsorbed water. *Sci. Rep.* **2016**, *6*, 35605. [CrossRef] [PubMed]

46. Deng, Y.; Gao, B.; Deng, M.; Luo, Y. A comparative theoretical study on core-hole excitation spectra of azafullerene and its derivatives. *J. Chem. Phys.* **2014**, *140*, 124304. [CrossRef] [PubMed]

47. Momma, K.; Izumi, F. VESTA: A three-dimensional visualization system for electronic and structural analysis. *J. Appl. Crystallogr.* **2008**, *41*, 653–658. [CrossRef]

48. Mohammadi, M.D.; Abdullah, H.Y.; Louis, H.; Etim, E.E.; Edet, H.O. Evaluating the detection potential of $C_{59}X$ fullerenes (X= C, Si, Ge, B, Al, Ga, N, P, and As) for H_2SiC_{12} molecule. *J. Mol. Liq.* **2023**, *387*, 122621. [CrossRef]

49. Sood, P.; Kim, K.C.; Jang, S.S. Electrochemical and electronic properties of nitrogen doped fullerene and its derivatives for lithium-ion battery applications. *J. Energy Chem.* **2018**, *27*, 528–534. [CrossRef]

50. Nattagh, F.; Hosseini, S.; Esrafili, M.D. Effects of B and N doping/codoping on the adsorption behavior of C_{60} fullerene towards aspirin: A DFT investigation. *J. Mol. Liq.* **2021**, *342*, 117459. [CrossRef]

51. Käämbre, T.; Qian, L.; Rubensson, J.-E.; Guo, J.-H.; Såthe, C.; Nordgren, J.; Palmqvist, J.-P.; Jansson, U. Study of oxygen-C_{60} compound formation by NEXAFS and RIXS. *Eur. Phys. J. D* **2001**, *16*, 357–360. [CrossRef]

52. Schulte, K.; Wang, L.; Moriarty, P.; Prassides, K.; Tagmatarchis, N. Resonant processes and Coulomb interactions in $(C_{59}N)_2$. *J. Chem. Phys.* **2007**, *126*, 184707. [CrossRef] [PubMed]

53. Tan, Z.; Zhang, D.; Tian, H.-R.; Wu, Q.; Hou, S.; Pi, J.; Sadeghi, H.; Tang, Z.; Yang, Y.; Liu, J.; et al. Atomically defined angstrom-scale all-carbon junctions. *Nat. Commun.* **2019**, *10*, 1748. [CrossRef] [PubMed]

54. Wang, S.; Zhao, R.; Zheng, T.; Lu, Z.; Fang, Y.; Xie, H.; Wang, W.; Xue, W. Rational Design of a Low-Dimensional and Metal-free Heterostructure for Efficient Water Oxidation: DFT and Experimental Studies. *Langmuir* **2022**, *38*, 12562–12569. [CrossRef]

55. Wohlers, M.; Werner, H.; Herein, D.; Schedel-Niedrig, T.; Bauer, A.; Schlögl, R. Reaction of C_{60} and C_{70} with molecular oxygen. *Synth. Met.* **1996**, *77*, 299–302. [CrossRef]

56. Frisch, M.J.; Schlegel, H.B.; Scuseria, G.E.; Robb, M.A.; Scalmani, G.; Barone, V.; Petersson, G.A.; Li, X.; Caricato, M.; Marenich, A.V.; et al. *Gaussian 16, Revision A.03*; Gaussian Inc.: Wallingford, CT, USA, 2016.

57. Triguero, L.; Pettersson, L.; Ågren, H. Calculations of near-edge X-ray-absorption spectra of gas-phase and chemisorbed molecules by means of density-functional and transition-potential theory. *Phys. Rev. B* **1998**, *58*, 8097. [CrossRef]

58. Delesma, F.A.; Van den Bossche, M.; Grönbeck, H.; Calaminici, P.; Köster, A.M.; Pettersson, L.G. A chemical view on X-ray photoelectron spectroscopy: The ESCA molecule and surface-to-bulk XPS shifts. *ChemPhysChem* **2018**, *19*, 169–174. [CrossRef]

59. Hua, W.; Gao, B.; Luo, Y. First-principle simulation of soft X-ray spectroscopy. *Prog. Chem.* **2012**, *24*, 964.

60. Nyberg, M.; Luo, Y.; Triguero, L.; Pettersson, L.G.; Ågren, H. Core-hole effects in x-ray-absorption spectra of fullerenes. *Phys. Rev. B* **1999**, *60*, 7956. [CrossRef]

61. Bassan, A.; Nyberg, M.; Luo, Y. Identifying isomers of C_{78} by means of x-ray spectroscopy. *Phys. Rev. B* **2002**, *65*, 165402. [CrossRef]

62. Gao, B.; Liu, L.; Wang, C.; Wu, Z.; Luo, Y. Spectral identification of fullerene C_{82} isomers. *J. Chem. Phys.* **2007**, *127*, 164314. [CrossRef] [PubMed]

63. Brena, B.; Luo, Y. Electronic structures of azafullerene $C_{48}N_{12}$. *J. Chem. Phys.* **2003**, *119*, 7139–7144. [CrossRef]

64. Qi, J.; Hua, W.; Gao, B. Theoretical study of two I_h-symmetry-breaking C_{60} isomers and their chlorinated species in core-excited and ground states. *Chem. Phys. Lett.* **2012**, *539*, 222–228. [CrossRef]

65. Pettersson, L.G.; Wahlgren, U.; Gropen, O. Effective core potential parameters for first-and second-row atoms. *J. Chem. Phys.* **1987**, *86*, 2176–2184. [CrossRef]

66. Becke, A.D. Density-functional exchange-energy approximation with correct asymptotic behavior. *Phys. Rev. A* **1988**, *38*, 3098. [CrossRef] [PubMed]

67. Perdew, J.P. Density-functional approximation for the correlation energy of the inhomogeneous electron gas. *Phys. Rev. B* **1986**, *33*, 8822. [CrossRef] [PubMed]

68. Hermann, K.; Pettersson, L.; Casida, M.; Daul, C.; Goursot, A.; Koester, A.; Proynov, E.; St-Amant, A.; Salahub, D.R.; Carravetta, V.; et al. *StoBe-deMon v.3.3*; Royal Institute of Technology: Stockholm, Sweden; Berlin, Germany, 2014.

69. Vall-Llosera, G.; Gao, B.; Kivimäki, A.; Coreno, M.; Ruiz, J.; de Simone, M.; Ågren, H.; Rachlew, E. The C 1s and N 1s near edge x-ray absorption fine structure spectra of five azabenzenes in the gas phase. *J. Chem. Phys.* **2008**, *128*, 044316. [CrossRef]

70. Gao, B.; Jiang, J.; Liu, K.; Luo, Y. *Bionano-Lego, Version 2.0*; Royal Institute of Technology: Stockholm, Sweden, 2008.

71. Brena, B.; Carniato, S.; Luo, Y. Functional and basis set dependence of K-edge shake-up spectra of molecules. *J. Chem. Phys.* **2005**, *122*, 184316. [CrossRef]

72. Brena, B.; Luo, Y.; Nyberg, M.; Carniato, S.; Nilson, K.; Alfredsson, Y.; Åhlund, J.; Mårtensson, N.; Siegbahn, H.; Puglia, C. Equivalent core-hole time-dependent density functional theory calculations of carbon 1s shake-up states of phthalocyanine. *Phys. Rev. B* **2004**, *70*, 195214. [CrossRef]

73. Brena, B.; Luo, Y. Time-dependent DFT calculations of core electron shake-up states of metal-(free)-phthalocyanines. *Radiat. Phys. Chem.* **2006**, *75*, 1578–1581. [CrossRef]

74. Gao, B.; Wu, Z.; Luo, Y. A density functional theory study of shake-up satellites in photoemission of carbon fullerenes and nanotubes. *J. Chem. Phys.* **2008**, *128*, 234704. [CrossRef]

75. Kutzelnigg, W.; Fleischer, U.; Schindler, M. The IGLO-method: Ab initio calculation and interpretation of NMR chemical shifts and magnetic susceptibilities. *Deuterium Shift Calc.* **1990**, *23*, 165–262.

76. Zhang, B.-B.; Lin, J.; Song, X.-N.; Wang, C.-K.; Hua, W.; Ma, Y. Identification of oxidation states in γ-graphyne by computational XPS and NEXAFS spectra. *Appl. Surf. Sci.* **2023**, *609*, 155134. [CrossRef]

77. Ming, J.; Zhang, J.-R.; Song, X.-N.; Li, X.; Hua, W.; Ma, Y. First-principles simulation of X-ray spectra of graphdiyne and graphdiyne oxides at the carbon K-edge. *Phys. Chem. Chem. Phys.* **2023**, *25*, 32421–32429. [CrossRef] [PubMed]